International Journal of Heat and Mass Transfer 52 (2009) 839–850

Contents lists available at ScienceDirect

International Journal of Heat and Mass Transfer

journal homepage: www.elsevier.com/locate/ijhmt

Effects of Reynolds and Prandtl numbers on heat transfer from a square cylinder in the unsteady flow regime

Akhilesh K. Sahu [a], R.P. Chhabra [a,*], V. Eswaran [b]

[a] Department of Chemical Engineering, Indian Institute of Technology, Kanpur 208 016, India
[b] Department of Mechanical Engineering, Indian Institute of Technology, Kanpur 208 016, India

ARTICLE INFO

Article history:
Received 31 October 2007
Received in revised form 21 July 2008
Available online 26 September 2008

Keywords:
Square cylinder
Unsteady flow
Prandtl number
Nusselt number
Strouhal number

ABSTRACT

The effects of the Reynolds and Prandtl numbers on the rate of heat transfer from a square cylinder are investigated numerically in the unsteady two-dimensional periodic flow regime, for the range of conditions $60 \leqslant Re \leqslant 160$ and $0.7 \leqslant Pr \leqslant 50$ (the maximum value of Peclet number being 4000). A semi-explicit finite volume method has been used on a non-uniform collocated grid arrangement to solve the governing equations. Using the present numerical results, simple heat transfer correlations are obtained for the constant temperature and constant heat flux conditions on the solid square cylinder. In addition, the variation of the time averaged local Nusselt number on the each face of the obstacle and representative isotherm plots are presented to elucidate the role of Prandtl number on heat transfer in the unsteady flow regime.

1. Introduction

The cross-flow and heat transfer from bluff bodies represents a problem of both considerable theoretical and practical significance. The flow over a circular cylinder represents one of the classical problems in fluid mechanics and a satisfactory understanding of the associated rich variety of flow phenomena is of intrinsic interest for the overall picture of bluff body fluid dynamics. On the other hand, such model flows also represent an idealisation of several industrially important flows; typical examples include flow in tubular and in pin-type heat exchangers, the use of thin cylinders as measuring probes and sensors, in the design of support structures and flow dividers in polymer processing applications, etc. Further applications are found in the continuous thermal treatment of food particles (such as slices and chips of carrots and potatoes) in viscous fluids (high Prandtl number) wherein not only the rate of heat transfer to particles is important, but a knowledge of the detailed temperature field is also vital to ensure uniform product quality [1–3]. The most commonly studied shapes include cylinders of circular and square cross-sections. While there is a great degree of commonality between these two geometries, they also differ significantly in a number of ways. Firstly, both configurations exhibit substantial wake regions and the flow induced unsteadiness which lead to improved mixing and enhanced rates of heat/mass transfer between the obstacle and the fluid. The two configurations also exhibit qualitatively similar instabilities characteristics, but the mechanisms of flow separation and the scaling of the vortex shedding frequency with the Reynolds number in the two cases are quite different. Furthermore, the separation points are fixed at the corners for a square cylinder, unlike in the case of a circular cylinder where the separation point keeps moving forward with the increasing Reynolds number. Thus, the square shape is more of a bluff body than the circular shape. In view of the foregoing, over the years, a significant amount of information dealing with different aspects of the flow and heat transfer, including the transition from one regime to another, wake characteristics, global flow and heat transfer parameters, wall effects, etc. has been added to the literature, a great majority of these studies relating to the flow over a circular cylinder (e.g., see Zdravkovich [4,5]). More recently, heat transfer results for the flow of air over an isothermal circular cylinder in unsteady laminar flow regime have been presented by Baranyi [6]. The heat transfer characteristics from a circular cylinder in steady flow regime has extensively studied by Bharti et al. [7] for the Prandtl number varying from 0.7 to 400. Similarly, a study in steady flow regime for two circular cylinders in tandem arrangement at four different Prandtl numbers 0.1, 1, 10 and 100 has been reported recently by Juncu [8]. Evidently, an improved understanding of the basic flow and thermal fields will lead to sound process engineering design and operations.

In contrast, the corresponding body of knowledge for a square cylinder is much less extensive. Since thorough accounts of the pertinent literature have been presented elsewhere recently (Sharma and Eswaran [9], Dhiman et al. [10,11]), only the salient points and the subsequent studies are detailed here, with a special reference to the 2D, unsteady flow regime for an unconfined cylinder.

* Corresponding author. Tel.: +91 512 259 7393; fax: +91 512 259 0104.
E-mail address: chhabra@iitk.ac.in (R.P. Chhabra).

0017-9310/$ - see front matter © 2008 Elsevier Ltd. All rights reserved.
doi:10.1016/j.ijheatmasstransfer.2008.07.032

Nomenclature

B	side of the square cylinder (m)
C_D	drag coefficient; $C_D = F_D/\frac{1}{2}\rho u_\infty^2 B$
C_p	specific heat of the fluid (J/kg K)
F_D	drag force per unit length of cylinder (N/m)
h	local convective heat transfer coefficient (W/m^2 K)
j_h	Colburn factor for heat transfer (Eq. (11))
k	thermal conductivity of the fluid (W/m K)
L	length of the computational domain (m)
H	height of the computational domain (m)
n	unit normal vector on the surface of the cylinder
M	number of grid points in the x-direction
N	number of grid points in the y-direction
Nu	Nusselt number; $Nu = hB/k$
p	pressure; $p = p'/\rho u_\infty^2$
Pe	Peclet number; $Pe = Re \times Pr$
Pr	Prandtl number; $Pr = c_p\mu/k$
q_w	constant heat flux on the surface of the cylinder (W/m^2)
Re	Reynolds number; $Re = Bu_\infty\rho/\mu$
S	surface of domain
t	time; $t = t'/(B/U_\infty)$
T	dimensionless temperature; $T = \left(\frac{T'-T_w}{T_w-T_\infty}\right)$ or $\left(\frac{T'-T_w}{q_w B/k}\right)$
u	component of the velocity in x-direction; $u = u'/u_\infty$
U_c	average dimensionless stream-wise velocity
v	component of the velocity in y-direction; $v = v'/u_\infty$
x	stream-wise coordinate; $x = x'/B$
L_D	downstream face distance of the cylinder from the outlet (m)
L_U	upstream face distance of the cylinder from the inlet (m)
y	transverse coordinate; $y = y'/B$

Greek symbols

β	blockage ratio, $\beta = B/H$
δ	size of the CV clustered around the cylinder (m)
Δ	size of the CV far away from the cylinder in x-direction (m)
ε	rate of deformation tensor
μ	viscosity of the fluid (Pa s)
Ω	volume of domain
ϕ	dependent variable in convective boundary condition
ρ	density of the fluid (kg/m^3)
τ	extra stress tensor (Pa)

Subscripts

∞	inlet condition
c	cylinder
f	front face of the square cylinder
r	rear face of the square cylinder
t	top face of the square cylinder
w	surface of the square cylinder

Superscript

$'$	dimensional variable

Broadly speaking for an unconfined square cylinder, the flow remains attached to the cylinder up to about $Re \leqslant 1$ and then it transits to the so-called (two-dimensional) steady symmetric flow which is characterized by the formation of a wake in the rear of the obstacle. This flow pattern persists up to about $Re = 40$ and with the further increase in the value of the Reynolds number, the symmetry of the flow about the mid-plane is destroyed. Though the flow is still two dimensional but it is no longer steady, as the vortex shedding occurs under these conditions. This regime continues up to about $Re = 200$ before making way for the onset of three-dimensional flow. This work is concerned with the two-dimensional unsteady flow regime, the maximum Reynolds number being limited to $Re = 160$. It is now readily agreed that while the flow and temperature fields in the steady and unsteady regimes can differ significantly, the time-averaged values of the global parameters like drag coefficient and Nusselt number are relatively insensitive to the time-dependent nature of the flow (Kelkar and Patankar [12], Sharma and Eswaran [9]), at least for the flow of air, i.e., a Prandtl number value of 0.7. Similarly, some investigators have studied the role of confinement on flow and heat transfer from a square cylinder placed in a channel in forced and mixed convection regimes (Turki et al. [13], Rahnama and Hadi-Moghaddam [14]). A few, e.g., Bhattacharyya and Mahapatra [15] have studied the effect of buoyancy on vortex shedding and heat transfer characteristics. It needs to be emphasized here that most of these studies have not only dealt with the case of an isothermal square cylinder, but are also restricted to a single value of the Prandtl number (usually air). Ji et al. [16] have done experiments with air to show the effect of flow pulsation on the heat transfer from a uniformly heated square cylinder in a channel for two values of Reynolds number 350 and 540 and three different blockage ratios 1/10, 1/8 and 1/6. In an extensive study, Sharma and Eswaran [9] investigated the flow and heat transfer characteristics from a square cylinder in the steady and unsteady flow regimes up the Reynolds number values of 160 isothermal and constant heat flux boundary conditions on the surface of the square cylinder, but again only for air.

However, many liquids encountered in chemical, petroleum and process engineering applications have Prandtl number values in the range of 50–100 and clearly the aforementioned results for air cannot be extrapolated to such large values of Prandtl numbers. From a numerical standpoint, the thermal boundary layer thins with the increasing values of the Prandtl number and therefore very fine grids are needed to resolve the flow satisfactorily under these conditions. The effect of the Prandtl number on the heat transfer from unconfined and confined square cylinders has been studied only recently by Paliwal et al. [17], Gupta et al. [18] and Dhiman et al. [10,11], but are limited to the steady flow regime ($Re \leqslant 40$). The heat transfer coefficient showed the usual scaling with $Pr^{1/3}$ up to about $Pr = 100$. On the other hand, many investigators have reported experimental results on heat transfer from cylinders to fluids with high values of the Prandtl numbers. The oft-quoted correlation of Whitaker [19] which brings together the experimental results from various studies, and for various geometries, unfortunately does not include the case of a square cylinder. In view of the new experimental results, this correlation has been re-visited recently by Sanitjai and Goldstein [20] who presented a new correlation which is claimed to offer a degree of improvement over the original equation of Whitaker [19].

From the foregoing description, it is perhaps safe to conclude that no prior numerical results are available on the role of Prandtl number on the rate of heat transfer from a square cylinder in the unsteady flow regime. This study aims to fill this gap in the literature. In particular, extensive numerical results are presented for an unconfined square cylinder over the following ranges of conditions $60 \leqslant Re \leqslant 160$ and $0.7 \leqslant Pr \leqslant 50$. In addition to the detailed results on the time-dependent behaviour of the Nusselt number, the time-averaged values for the individual surfaces of the cylinder and from

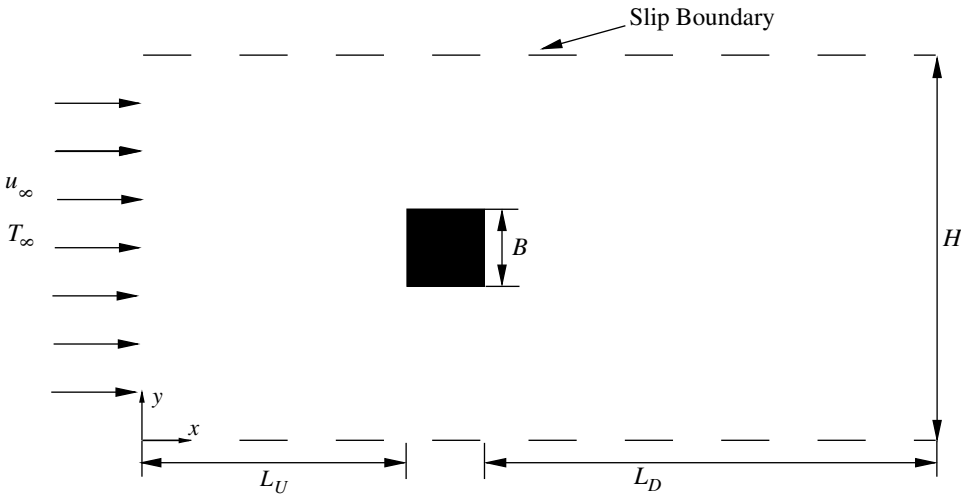

Fig. 1. Schematics of the flow around a square cylinder.

the whole cylinder are discussed and correlated with the Reynolds and Prandtl numbers.

2. Problem statement and mathematical formulation

The physical problem considered in this study is the two-dimensional flow of an incompressible flow around a square cylinder placed in an uniform stream having velocity u_∞ and temperature T_∞ (Fig. 1). In order to make the problem computationally tractable, the square cylinder is located symmetrically in between two artificial confining walls which are assumed to be free-slip surfaces thereby exerting very little influence on the velocity and temperature fields near the cylinder. The ratio of the width of the cylinder, B, to that of the confining walls, H defines the blockage ratio ($\beta = B/H$) for a confined flow. Extensive studies [e.g., see 9] have shown that the confining boundaries have very little effect on the characteristics of the flow in the vicinity of the cylinder for $H = 20B$. Thus, this value has been used in the present work to simulate the unconfined flow condition. Similarly, based on the extensive numerical experimentation [9–11], the non-dimensional distance between the inlet plane and the front surface of the cylinder, L_U, is 8.5, and that between the rear surface of the cylinder and the exit plane, L_D, is 16.5, with the total non-dimensional length of the computational domain in the axial direction, $L = 26$. The surface of the square cylinder is assumed to be subjected to either a constant wall temperature T_w or an uniform heat flux q_w. The thermo-physical properties are assumed to be independent of temperature and further there is no viscous dissipation [21]. Under these conditions, the integral forms of the equations of continuity, momentum and thermal energy in their non-dimensional forms are written as follows:

Continuity:

$$\int_s \mathbf{V}\cdot d\mathbf{S} = 0 \tag{1}$$

x-Momentum:

$$\frac{\partial}{\partial t}\int_\Omega u\,d\Omega + \int_S u\mathbf{V}\cdot d\mathbf{S} = -\int_S p\hat{i}\cdot d\mathbf{S} + \frac{2}{Re}\int_S\left(\varepsilon_{xx}\hat{i}+\varepsilon_{xy}\hat{j}\right)\cdot d\mathbf{S} \tag{2}$$

y-Momentum:

$$\frac{\partial}{\partial t}\int_\Omega v\,d\Omega + \int_S v\mathbf{V}\cdot d\mathbf{S} = -\int_S p\hat{j}\cdot d\mathbf{S} + \frac{2}{Re}\int_S\left(\varepsilon_{yx}\hat{i}+\varepsilon_{yy}\hat{j}\right)\cdot d\mathbf{S} \tag{3}$$

Energy equation:

$$\frac{\partial}{\partial t}\int_\Omega T\,d\Omega + \int_\Omega T\mathbf{V}\cdot d\mathbf{S} = -\frac{1}{RePr}\int_S\left(\frac{\partial T}{\partial x}\hat{i}+\frac{\partial T}{\partial y}\hat{j}\right)\cdot d\mathbf{S} \tag{4}$$

where $d\mathbf{S}$ equals $\mathbf{n}\,dS$ ($\mathbf{n}$ is the unit normal vector to the surface dS) and $\hat{i},\hat{j}$ are the unit vectors in the x- and y-directions, respectively. For an incompressible fluid, the stress tensor is related to the components of the rate of deformation tensor, ε as

$$\tau_{ij} = 2\eta\varepsilon_{ij} \quad \text{where} \quad \varepsilon_{ij} = \frac{1}{2}(\partial_j V_i + \partial_i V_j) \tag{5}$$

The field variables appearing in the aforementioned equations are rendered dimensionless using B, u_∞, B/u_∞ and ρu_∞^2 as scaling variables for length, velocity, time and pressure, respectively. The temperature is made dimensionless using $\left(\frac{T'-T_w}{T_w-T_\infty}\right)$ for the constant wall temperature case or $\left(\frac{T'-T_w}{q_w B/k}\right)$ for the uniform heat flux condition.

The two dimensionless groups, Reynolds and the Prandtl numbers, appearing in Eqs. (2)–(4) are defined as:

$$Re = \frac{\rho u_\infty B}{\mu} \tag{6}$$

$$Pr = \frac{c_p\mu}{k} \tag{7}$$

The physically realistic boundary conditions (in their dimensionless form) for this flow are:

- At inlet boundary
  $u = 1, \quad v = 0, \quad T = 0$
- At upper and lower bounding walls
  $\frac{\partial u}{\partial y} = 0, \quad v = 0, \quad \frac{\partial T}{\partial y} = 0$
- On the surface of the square cylinder
  $u = 0, \quad v = 0$

  case I: constant temperature case, $T = 1$ or
  case II: constant heat flux case, $\frac{\partial T}{\partial n} = -1$.
- At the exit boundary, the convective boundary condition given by $\frac{\partial\phi}{\partial t} + U_c\frac{\partial\phi}{\partial x} = 0$ has been used, with the average non-dimensional stream-wise velocity, $U_c = 1$ and ϕ is a dependent variable, u or v or T.

The numerical solution of Eqs. (1)–(4) along with the above-noted boundary conditions yields the velocity, pressure and temperature fields and these, in turn, are processed further to deduce the global characteristics like drag coefficients and Nusselt number. The local Nusselt number, Nu_x, is defined as (hB/k) and is evaluated using the temperature field as follows:

For the top and bottom faces of the cylinder:

$$Nu_x = \pm\frac{\partial T}{\partial y}\bigg|_{\mathrm{w}} \tag{8}$$

For the front and rear faces of cylinder:

$$Nu_y = \mp\frac{\partial T}{\partial x}\bigg|_{\mathrm{w}} \tag{9}$$

Eqs. (8) and (9) are applicable for the constant temperature condition at the solid cylinder. The analogous expression for the case of the constant heat flux condition is:

$$Nu_x = Nu_y = \frac{1}{T_{\mathrm{w}}} \tag{10}$$

for all the four faces of the cylinder, where T_{w} is the local fluid temperature at the respective wall. The local Nusselt number values are averaged over the whole cylinder to obtain the overall mean value of the Nusselt number which can be used in process engineering design calculations to estimate the rate of heat transfer from the cylinder or the temperature of the cylinder.

3. Numerical details

In the present work, the general finite volume method of Eswaran and Prakash [22] and of Sharma and Eswaran [23] initially developed for complex 3D geometries on a non-staggered grid has been used here in its simplified form for 2D flows. In brief, the semi-explicit method is used to solve the unsteady Navier–Stokes equations in which the momentum equations are discretized in an explicit manner, with the exception of pressure terms which are treated implicitly. Two steps are implemented at each time level: first, a predicted velocity is obtained from the discretized momentum equation using the previous time-level pressure field; the second corrector step consists of the iterative solution of the pressure-correction equation and in obtaining the corresponding velocity corrections such that the final velocity field satisfies the continuity equation to the prescribed limit. The convective terms are discretized using the QUICK [24] scheme while the diffusive terms are discretized using the central difference scheme. Similarly, the energy equation has been solved explicitly to obtain the unsteady temperature field using the calculated velocity field at each time level.

The grid structure used in the present work is shown in Fig. 2. The grid is divided into five separate zones in both directions, and uniform as well as nonuniform grid distributions are employed. The grid distribution was made uniform with a constant cell size, $\Delta = 0.25B$, outside a region around the cylinder that extended four units upstream, downstream and sideways. A grid of much smaller size δ, is clustered around the cylinder over a distance of 1.5 units to adequately capture wake–wall interactions in both directions. The hyperbolic tangent function has been used for stretching the cell sizes between these limits of δ and Δ.

In order to obtain reliable and accurate results, it is important to choose carefully the length and width of the computational domain and grid size. A thorough grid independence study for the problem under consideration has been done by Sharma and Eswaran [9] at $Re = 160$ and $Pr = 0.7$ and Dhiman et al. [11] at $Re = 45$ and $Pr = 50$. Based on these studies, in the present study, for the highest Reynolds number of 160 and Prandtl number of 20, five non-uniform grids (223×179, 246×200, 295×241, 325×271 and 365×303) were used to demonstrate the grid independence of the results, as shown in Fig. 3. The percentage change in the values of the pressure and total drag coefficients and the average Nusselt number for the coarsest grid ($M \times N = 223 \times 179$) and the finest grid ($M \times N = 365 \times 303$) are 3.3%, 3%, 2% (constant temperature case) and 2.5% (constant heat flux case), respectively. The

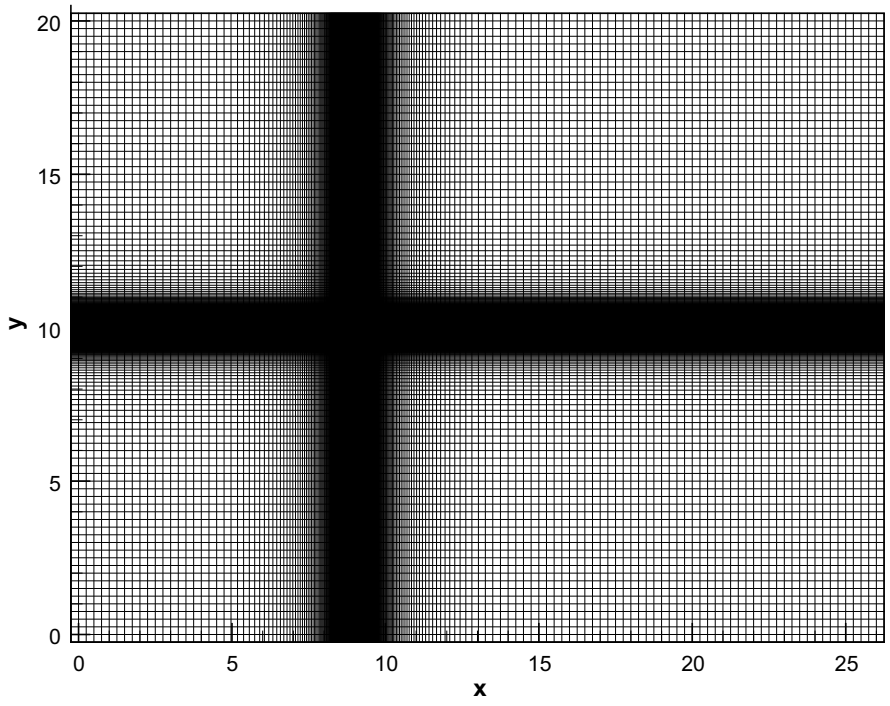

Fig. 2. Non-uniform computational grid with 325×271 grid points.

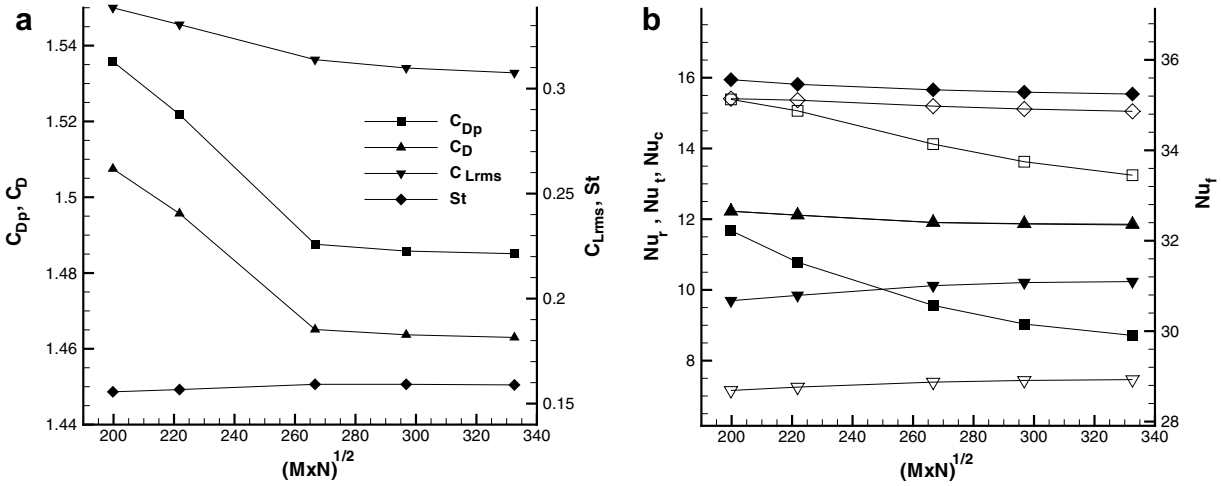

Fig. 3. Grid independence results at $Re = 160$ and $Pr = 20$ for the (a) flow parameters and (b) average Nusselt number for the cylinder and each of its faces with both types of boundary conditions. Filled and open symbols correspond to the cases of constant cylinder temperature and constant heat flux, respectively, and the symbols □, △, ▽ and ◇ represent the front face, rear face, top face and cylinder, respectively.

corresponding percentage changes in the values of C_D and average Nusselt number between the last two grids sizes are only 0.05%, 0.4% (constant temperature case) and 0.3% (constant heat flux case), respectively. One can thus conclude that the 325×271 grid size is sufficiently refined to resolve the flow and heat transfer fields and it has been used in all further computations reported in this work. Based on the extensive experimentation by Sharma and Eswaran [9] and Dhiman et al. [11], the upstream face distance of the square cylinder from inlet, L_U, is taken at 8.5 and the downstream face distance of the cylinder from the outlet, L_D, is set at 16.5. The distance between the lower and upper slip boundaries, H, is kept at 20. These choices are consistent with the other contemporary studies available in the literature.

It has been generally reported that the stable periodic flow around a square cylinder at a given Reynolds number is independent of the initial conditions [9]; only the time to achieve the stable periodicity depends upon the initial conditions. In the present study, the calculations are started either from rest or from the converged flow field relating to the lower Reynolds number, Re. The time step is taken to be 8×10^{-4}. The use of smaller values of the time-step did not produce any significant change in the root mean square (rms) and average values of the lift and drag coefficients and of the Nusselt number.

The numerical method used here has been extensively validated and benchmarked by Sharma and Eswaran [9] for $Pr = 0.7$ in the unsteady flow regime and by Dhiman et al. [11] for the larger values of Prandtl number in the steady flow regime for a square cylinder. The present values of the key parameters including pressure drag, C_{Dp}, total drag, C_D, rms value of lift coefficient, C_{Lrms}, and the Strouhal number, St, in the unsteady flow regime are compared with those of Sharma and Eswaran [9] in Table 1. The heat transfer results for high Prandtl numbers in the steady flow regime are compared with that of Dhiman et al. [11] in Table 2. The excellent agreement seen in Tables 1 and 2 inspires confidence in the use of this solver to study the effect of the Reynolds and Prandtl numbers on heat transfer from an unconfined square cylinder in the 2D unsteady flow regime.

4. Results and discussion

Numerical computations have been carried out for $Re = 60$–160 in step of 20 and for a range of values of the Prandtl number varying from 0.7 to 50 for the two thermal boundary conditions. However, the maximum value of the Peclet number $Pe = Re \times Pr$ is limited to 4000; i.e., $Pe \leqslant 4000$ and therefore the range of Prandtl number Pr is linked to the value of Reynolds number Re. This flow is characterized by six dimensionless groups, namely, drag coefficient, Nusselt number, lift coefficient, Reynolds number, Prandtl number and Strouhal number together with the type of thermal condition. While the fluid mechanical aspects including the drag and lift characteristics have been studied extensively by Sharma and Eswaran [9], the effect of Prandtl number on the heat transfer is explored here. It is appropriate to add here that prior to obtaining the instantaneous and time-averaged thermal fields that were used for the calculation of the heat transfer parameters, the unsteady computations were carried out at least for 20 cycles after the asymptotic shedding frequency of the Karman vortex had been reached. This was done to ensure that the fully periodic regime was attained.

Table 1
Comparison of the C_{Dp}, C_D, C_{Lrms} and St at $Re = 60$, 100 and 160 with the literature value

Re	Source	C_{Dp}	C_D	C_{Lrms}	St
40	Present study	1.5112	1.7612	–	–
	Sharma and Eswaran [9]	1.5130	1.7649	–	–
60	Present study	1.4525	1.5994	0.0907	0.1269
	Sharma and Eswaran [9]	1.4557	1.6032	0.0914	0.1271
100	Present study	1.4410	1.4878	0.1880	0.1486
	Sharma and Eswaran [9]	1.4462	1.4936	0.1922	0.1488
160	Present study	1.4831	1.4613	0.3066	0.1598
	Sharma and Eswaran [9]	1.4896	1.4681	0.3183	0.1596

Table 2
Comparison of the average Nusselt number with the literature value

Pr	Re	Present study	Dhiman et al. [11]	Sharma and Eswaran [9]
Constant wall temperature condition				
0.7	40	2.6967	2.6969	2.7071
	100	4.0254	–	4.0439
	160	2.6967	–	2.7071
100	40	14.5023	14.2351	–
Constant heat flux condition				
0.7	40	2.9785	2.9790	20.9894
	100	4.4185	–	4.4392
	160	5.3042	–	5.3436
100	40	17.9479	17.1410	–

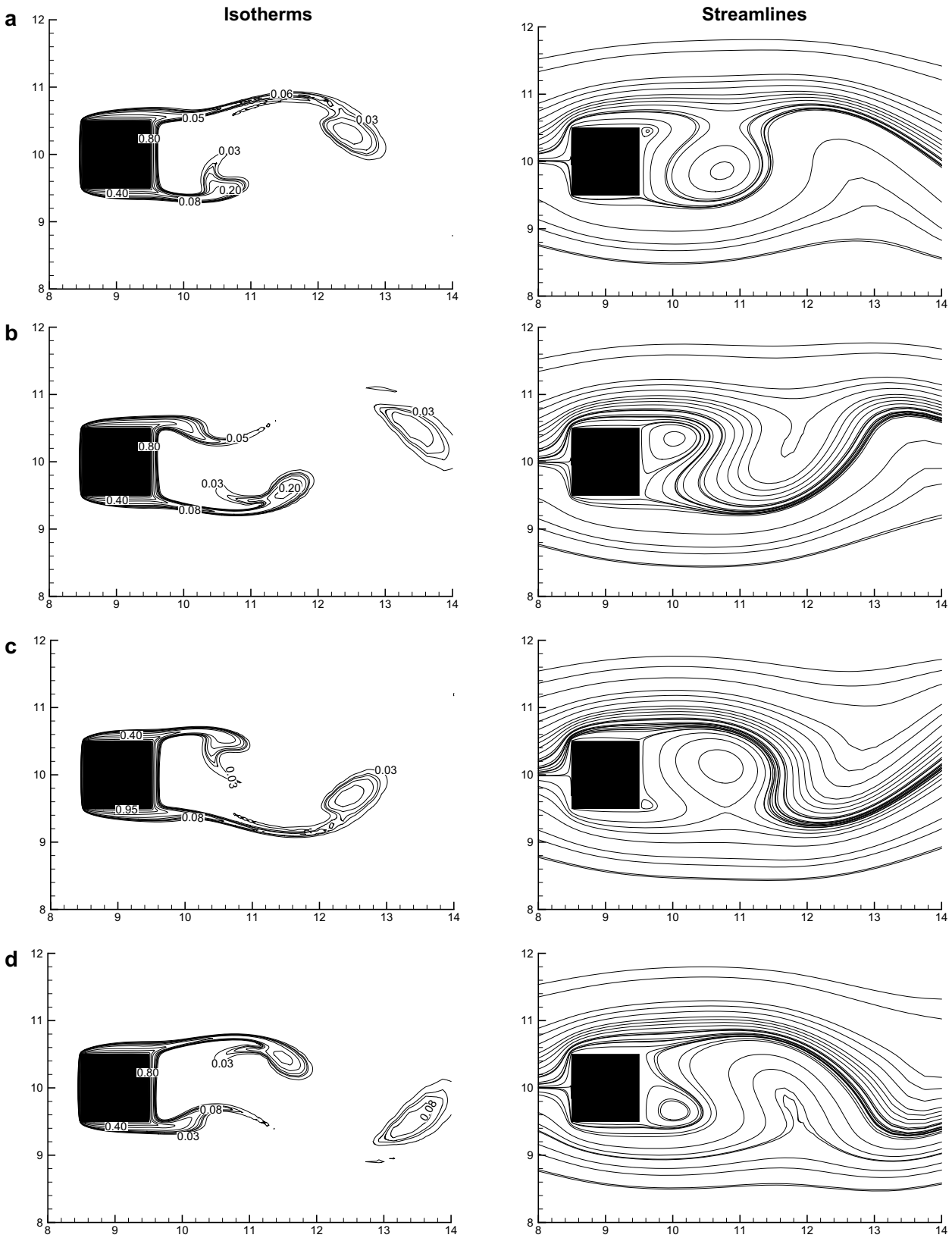

Fig. 4. Instantaneous isotherms for constant wall temperature condition and streamlines during one cycle of vortex shedding behind a square cylinder at $Re = 100$ and $Pr = 20$.

4.1. Isotherm patterns

Fig. 4(a)–(d) shows the instantaneous isotherms followed by the streamlines at four different times within a cycle of the periodic vortex shedding at $Re = 100$ and $Pr = 20$. The vortex is seen to be breaking off from the top of the rear face shown in Fig. 4(a) and (b) and subsequently from the bottom of the rear face (Fig. 4(c) and (d)). This alternate breaking off from the upper and lower sides gives rise to the periodic nature of the wake behind the cylinder.

Fig. 5 shows the representative time-averaged isotherm plots in the vicinity of the square cylinder for *Re* = 60, 100 and 160 at different Prandtl numbers. The isotherms for the constant temperature and constant heat flux cases are shown above and below the horizontal axis, respectively. The streamline representing the closed near-wake is also included in these figures as a thick line. It is seen from these figures that the front surface has the maximum crowding of the temperature contours, indicating the highest value of the Nusselt number, as compared to the other surfaces of the cylinder. It has been shown previously that an increase in the value of the Reynolds number leads to the clustering of isotherms near the cylinder [9]. This is so presumably due to the rolling of vortices close to the cylinder. An increase in Prandtl number also increases the crowding of isotherms. It can be seen in Fig. 5 that isotherms are confined to a smaller region at high values of the Prandtl number thereby suggesting the bulk of the resistance to heat transfer confined to a thin layer of fluid. This is clearly due to the thinning of the thermal boundary layer with the increasing Prandtl number.

4.2. Local Nusselt number

In this study, the local Nusselt number, *Nu*, is defined as $-\frac{\partial T}{\partial n}\big|_w$ and $\frac{1}{T_w}$ for the constant temperature and constant heat flux cases, respectively. The Nusselt number obtained here is the time-averaged over a certain integer number of cycles of vortex shedding.

4.2.1. Constant wall temperature case

A typical variation of the time-averaged local Nusselt for the top half of the square cylinder (the other half is symmetric) for the constant temperature condition at *Re* = 60 and at *Re* = 160 for different values of the Prandtl number is shown in Fig. 6(a) and (c). As expected, the Nusselt number increases with the increasing values of the Reynolds number and/or Prandtl number. Fig. 6 shows that the Nusselt number increases along the top half of the front face (AB) of cylinder and reaches its maximum value at the corner. For the top surface (BC), it has a local minimum due to the turning of the isotherms near the trailing edge of the cylinder. In the separated flow region (CD), there is a weak local minimum near the corner of the cylinder for higher values of Prandtl number at *Re* = 60 and all values of Prandtl number used in this study at *Re* = 160. Fig. 5 shows that isotherms in the separated region move closer to each other as they approach the axis of symmetry, which results in an increase in the Nusselt number near the rear stagnation point.

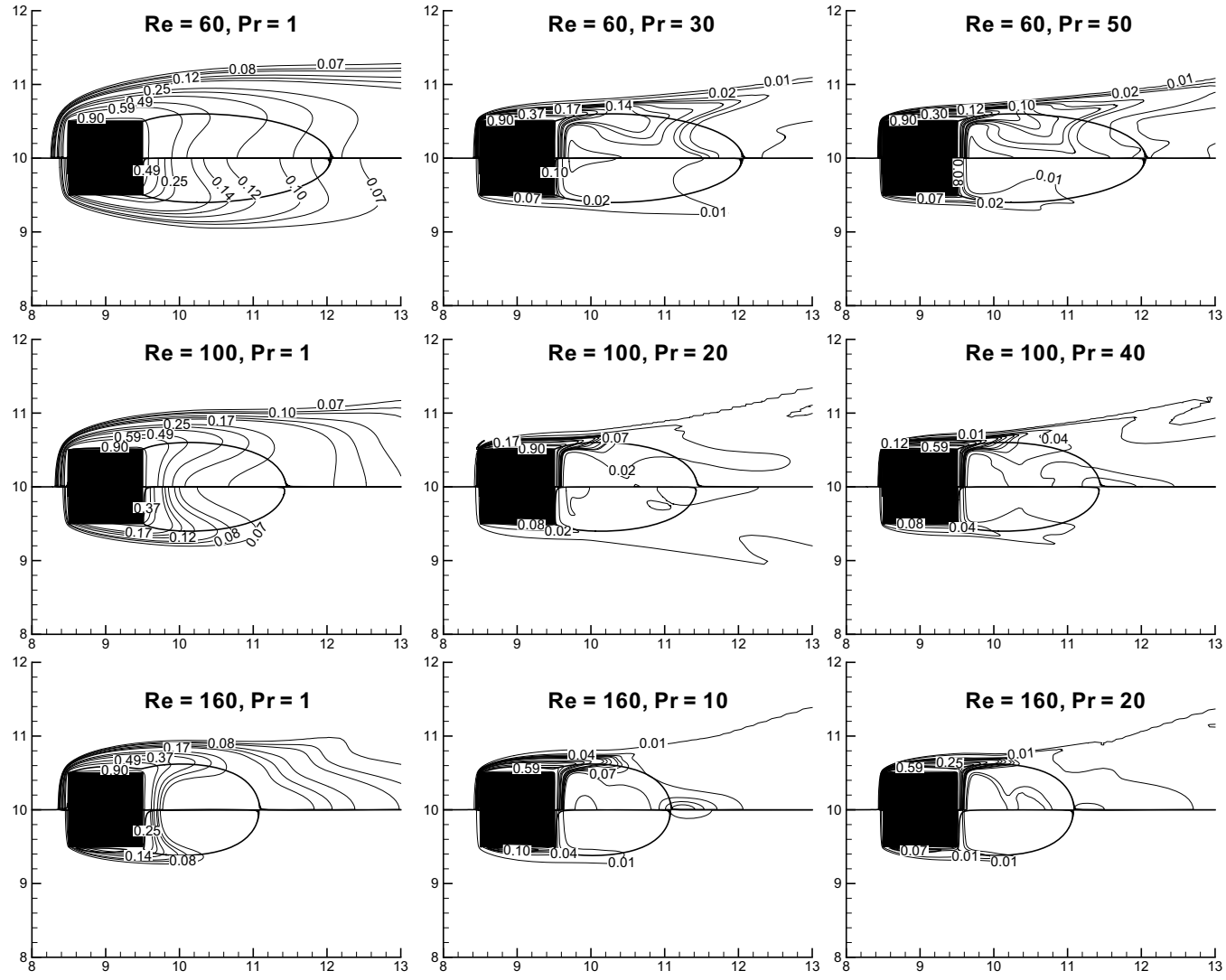

Fig. 5. The time averaged streamlines representing the closed near wake (shown by a thick line) and time averaged isotherms (upper and lower half present the results for constant wall temperature and constant heat flux cases, respectively) for *Re* = 60, 100 and 160 at different Prandtl numbers.

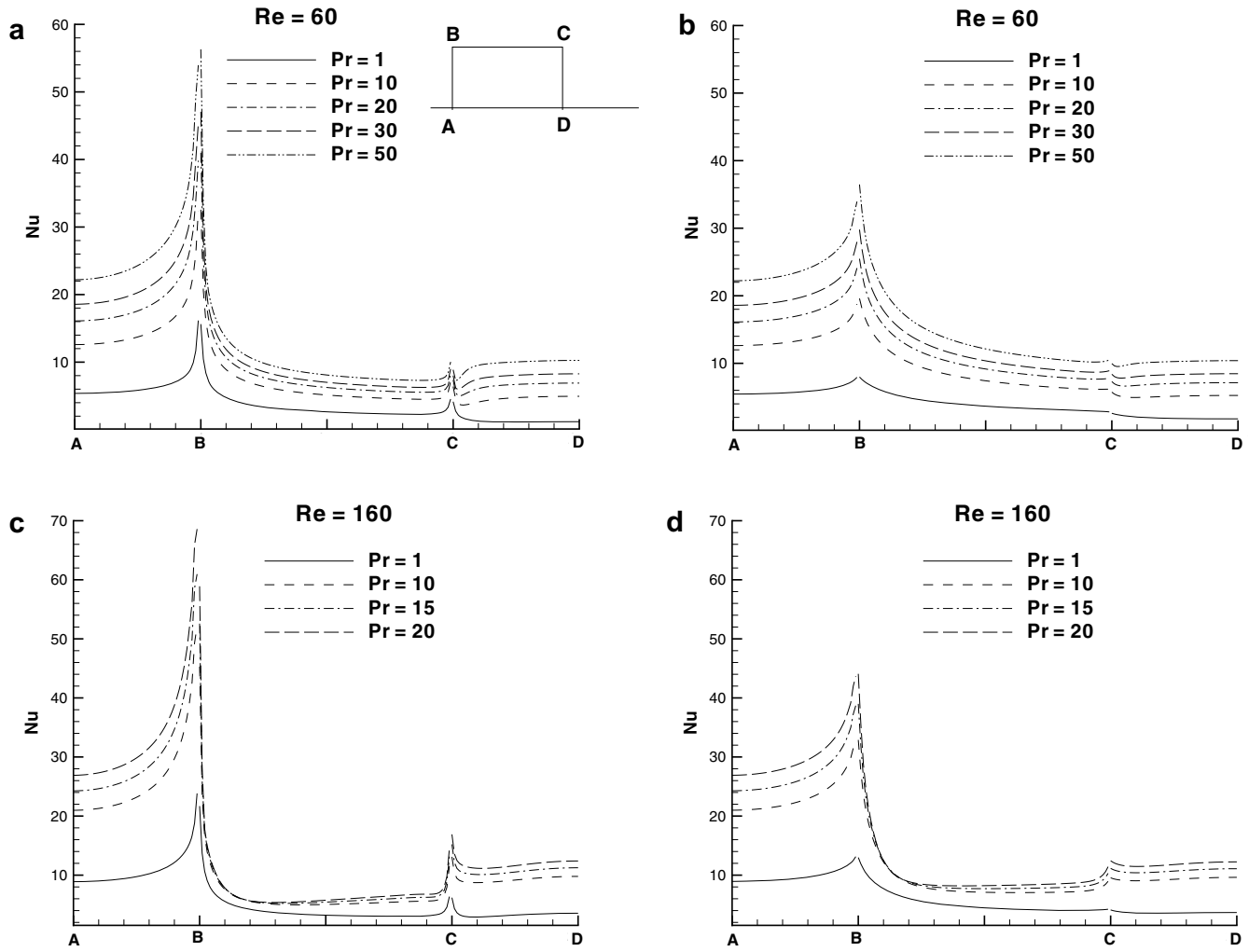

Fig. 6. Time-averaged Nusselt number distribution along the sides of the cylinder for *Re* = 60 and for *Re* = 160 at different Prandtl numbers for constant wall temperature (a) and (c) and constant heat flux (b) and (d) cases.

4.2.2. Constant heat flux case

The corresponding representative variation of the time-averaged local Nusselt for the top half of the square cylinder (the other half is symmetric) for the constant heat flux condition at *Re* = 60 and at *Re* = 160 for different Prandtl numbers is shown in Fig. 6(b) and (d). For this condition, the local Nusselt number at the top surface (BC) monotonically decreases from the leading to the trailing edge for all values of Prandtl number at *Re* = 60 and for higher values of Prandtl number at *Re* = 160, it has a minimum value near the corner of the cylinder. For the both front and rear surfaces, the variation in the local Nusselt number is seen to be qualitatively similar to that seen for the constant temperature condition case. However, the quantitative values in the two cases are quite different, as is to be expected given that the Nusselt number itself is defined differently in the two cases.

4.3. Average Nusselt number

The average Nusselt number for each surface of the square cylinder is obtained by averaging the time averaged local Nusselt number over the cylinder surfaces. The overall average Nusselt number is obtained by further averaging these values for each surface of the cylinder. Since the heat transfer area is the same for each surface of the square cylinder, this is simply the mean of the surface averaged values of the Nusselt number.

The variation of the surface average Nusselt number at each of the four sides of the cylinder with Reynolds number and Prandtl number is shown in Fig. 7. The front surface has the highest value of the Nusselt number, followed by the top/bottom or the rear surface depending upon the value of the Prandtl and/or of the Reynolds number. At high Reynolds and Prandtl numbers, the rear surface has a high value of the Nusselt number, as seen in Fig. 6 where the middle curve is at lower level than the last curve. This is due to the thinning of the thermal boundary layer at the rear surface at high Reynolds and Prandtl numbers, shown in Fig. 5. These results further show that the front surface, the rear surface and the cylinder average Nusselt numbers increase with the Reynolds and Prandtl numbers whereas the top or bottom surface values show a local maximum at higher values of Reynolds and Prandtl number. It is further observed that the variation of the average Nusselt number with the Reynolds and Prandtl numbers is qualitatively similar for both types of thermal boundary conditions. As seen in the steady flow regime [11], here also the average Nusselt number is always higher for the constant heat flux condition than that for the constant wall temperature condition (although the *peak* Nusselt number is higher in the constant temperature case, see Fig. 6).

4.4. Time history

Some further insights can be gained by examining the variation of the Nusselt number and flow parameters with time. Representa-

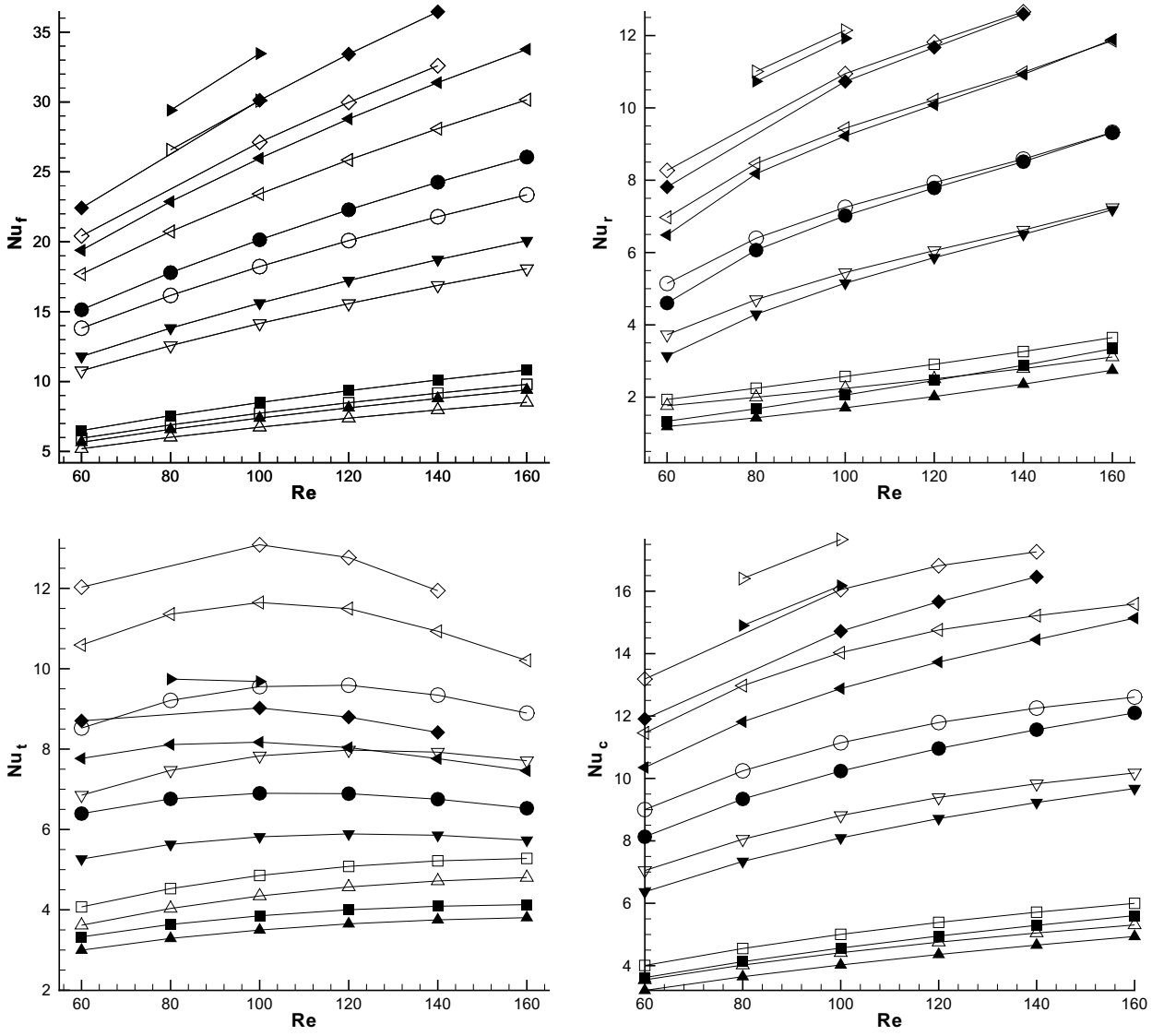

Fig. 7. Average Nusselt number for the overall cylinder and individual faces as a function of Reynolds number at different Prandtl numbers for constant temperature (filled symbols) and constant heat flux (opened symbols) cases (△, $Pr = 0.7$; □, $Pr = 1$; ▽, $Pr = 5$; ○, $Pr = 10$; ◁, $Pr = 20$; ◇, $Pr = 30$; and ▷, $Pr = 40$).

tive temporal variations of the flow and heat transfer parameters are shown in Fig. 8. The frequency of vortex shedding is estimated from the temporal variation of the lift coefficient and this is quantified in terms of a Strouhal number $\left(St = \frac{fB}{u_\infty}\right)$. Fig. 8(a) shows that the frequency of drag coefficient is twice of that of the lift coefficient. The temporal variation of the Nusselt number at each surface of the cylinder and of the total Nusselt number at $Re = 100$ and $Pr = 1$ is shown in Fig. 8(b). As expected, the Nusselt number at the top and bottom faces is found to be oscillating with the frequency of the lift coefficient whereas the total Nusselt number oscillates at the frequency of the drag coefficient (Fig. 8(c)). The frequency of the temporal variation of the rear and front surfaces Nusselt number is same as the frequency of the total Nusselt number. Fig. 8(b) and (c) shows that the amplitude of the temporal variation of the total, front and rear surface Nusselt numbers is very small. The effect of Prandtl number on the rate of heat transfer from the cylinder is shown in Fig. 8(d)–(f). As expected, an increase in the value of the Prandtl number enhances the rate of heat transfer at all Reynolds numbers.

From an application viewpoint, it is desirable to develop a simple correlating equation which can also be useful to interpolate the results for the intermediate values of the Reynolds and Prandtl numbers. Many authors have presented correlations for the Nusselt number as a function of the Prandtl and Reynolds numbers for circular [25,26] and for square cylinders [9]. For instance, Sharma and Eswaran [9] have proposed a correlation for the flow over a square cylinder for both these thermal boundary conditions for $Re = 5$–160 but for a single value of the Prandtl number, i.e., 0.7. Recently, Dhiman et al. [11] have modified this correlation in terms of the Colburn j_h factor and the Reynolds number over the range of conditions $5 \leqslant Re \leqslant 45$ and $0.7 \leqslant Pe \leqslant 4000$. The Colburn heat transfer factor j_h is defined as

$$j_h = \frac{Nu_c}{Re \times Pr^{1/3}} \tag{11}$$

The use of j_h factor, reconciles the results for a range of the Reynolds and Prandtl numbers on to a single curve. In the present work, it is observed (Fig. 9) that the j_h factor varies linearly with the Reynolds number for the range of conditions $60 \leqslant Re \leqslant 160$ and $0.7 \leqslant Pr \leqslant 50$ for the constant wall temperature and the constant heat flux conditions. The present numerical results are best described by the following fits:

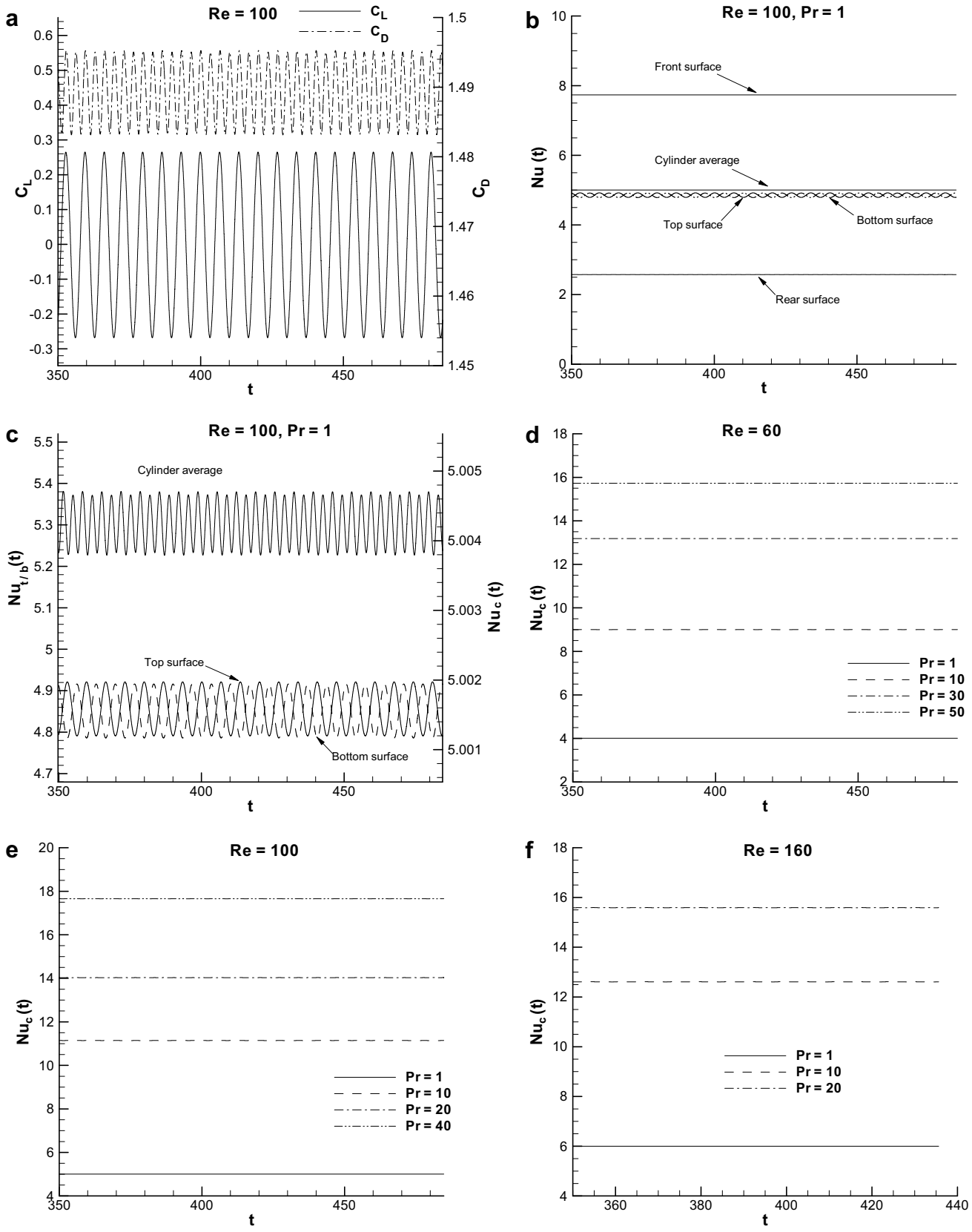

Fig. 8. Time distribution of flow parameters (C_D,C_L) and heat transfer parameters (Nu_c, Nu_f, Nu_r, Nu_t and Nu_b).

$$j_h = 0.706 \times Re^{-0.591} \quad (12)$$

for the constant wall temperature condition. Eq. (12) correlates the present numerical data (39 data points) with the maximum and average deviations of 4.34% and 1.60%, respectively. The corresponding expression for the constant heat flux condition is given by

$$j_h = 0.971 \times Re^{-0.642} \quad (13)$$

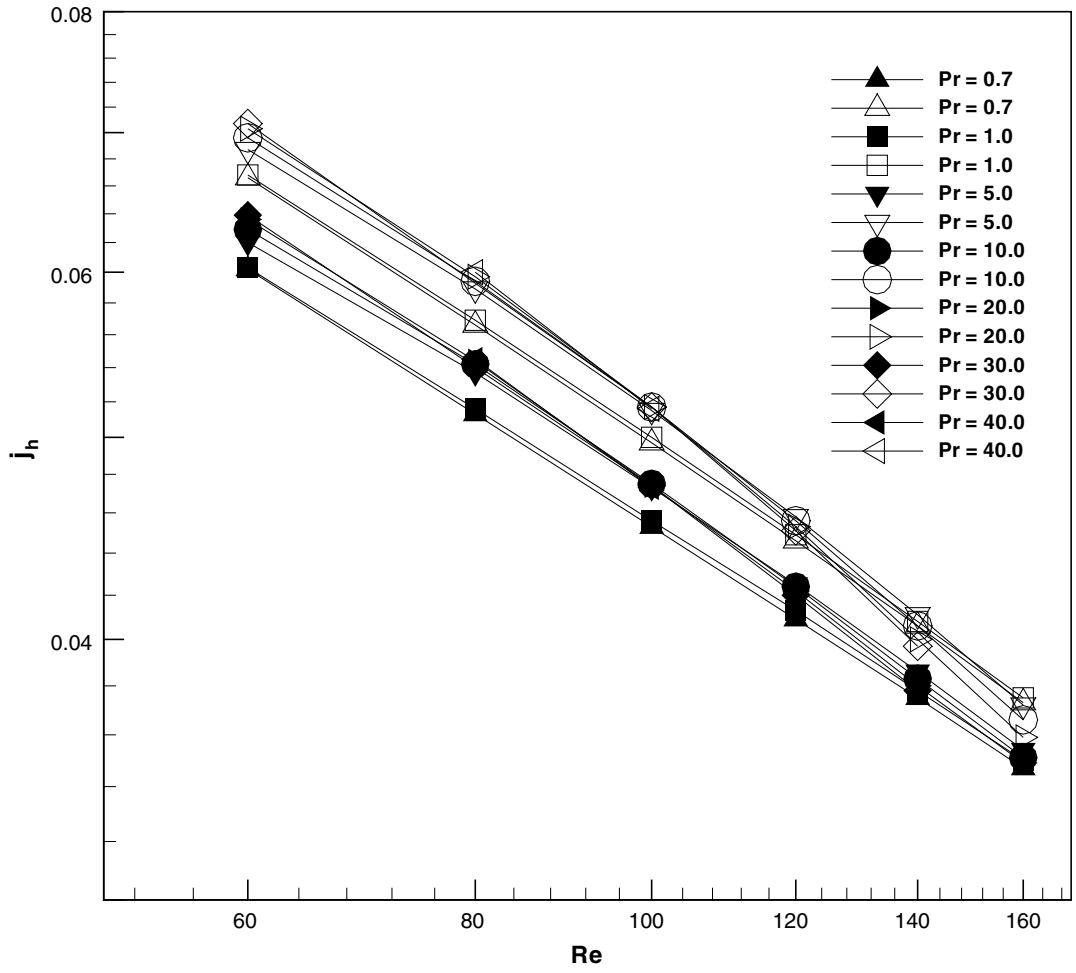

Fig. 9. The Colburn j_h factor as a function of Reynolds number at different Prandtl numbers for constant temperature (filled symbols) and constant heat flux (opened symbols) cases.

Eq. (13) has an average deviation of 1.7% which rises to a maximum of 5.12%.

In summary, this is the first numerical study in which the effect of the Prandtl number on the rate of heat transfer has been studied in this flow regime. The future studies will address the influence of the temperature-dependent physical properties and/or of the viscous dissipation on the overall heat transfer process. Until these results become available, it is suggested that these results can be modified by the usual empirical correction factor involving the ratio of the viscosities at the wall and the bulk conditions raised to a small power of 0.14 in case of fluids exhibiting strongly temperature-dependent viscosity. In any case, this correction is expected to be small.

5. Conclusions

A numerical study on the heat transfer from a heated square cylinder in the 2D unsteady cross-flow has been made for the range of conditions $60 \leqslant Re \leqslant 160$ and $0.7 \leqslant Pr \leqslant 50$ (the maximum value of Peclet number being 4000). The overall mean and surface averaged Nusselt numbers have been calculated for the two commonly used thermal boundary conditions, i.e., constant temperature and constant heat flux, prescribed on the surface of the cylinder. The present results show that the local Nusselt number over each face of the obstacle increases with an increase in the Reynolds and Prandtl numbers. Hence, the overall mean Nusselt number also increases with the Reynolds and Prandtl numbers. The Nusselt number profiles for the two boundary conditions are qualitatively similar, though the constant heat flux case has numerically higher mean *Nu*, for identical conditions. The front surface of the cylinder exhibits the highest value of the surface average Nusselt number. Due to the symmetry about mid-plane, the top and bottom surfaces have equal values of the local and average Nusselt numbers. The average value of the Nusselt number at the rear face, however, exceeds the values at the top or bottom surfaces at high Reynolds and Prandtl numbers. Finally, the numerical results obtained in this work are correlated in terms of the Colburn j_h factor which allows an easy estimation of the Nusselt number for the intermediate values of the Prandtl and Reynolds numbers.

References

[1] C.A. Lareo, P.J. Fryer, Vertical flows of solid–liquid mixtures, J. Food Eng. 36 (1998) 417–443.
[2] K.P. Sandeep, C.A. Zuritz, Residence times of multiple particles in non-Newtonian holding tube flow: effect of process parameters and development of dimensionless correlations, J. Food Eng. 25 (1) (1995) 31–44.
[3] K.P. Sandeep, C.A. Zuritz, V.M. Puri, Modelling two-phase flow in conventional and helical-holding tubes, Int. J. Food Sci. Technol. 35 (2000) 511–522.
[4] M.M. Zdravkovich, Flow Around Circular Cylinders: Fundamentals, vol. 1, Oxford University Press, New York, 1997.
[5] M.M. Zdravkovich, Flow Around Circular Cylinders: Applications, vol. 2, Oxford University Press, New York, 2003.
[6] L. Baranyi, Computation of unsteady momentum and heat transfer from a fixed circular cylinder in laminar flow, J. Comput. Appl. Mech. 4 (1) (2003) 13–25.

[7] R.P. Bharti, R.P. Chhabra, V. Eswaran, A numerical study of the steady forced convection heat transfer from an unconfined circular cylinder, Heat Mass Transfer 41 (2005) 824–833.
[8] G. Juncu, A numerical study of momentum and forced convection heat transfer around two tandem circular cylinders at low Reynolds numbers. Part II. Forced convection heat transfer, Int. J. Heat Mass Transfer 50 (2007) 3799–3808.
[9] A. Sharma, V. Eswaran, Heat and fluid flow across a square cylinder in the two-dimensional laminar flow regime, Numer. Heat Transfer A 45 (3) (2004) 247–269.
[10] A.K. Dhiman, R.P. Chhabra, V. Eswaran, Flow and heat transfer across a confined square cylinder in the steady flow regime: effect of Peclet number, Int. J. Heat Mass Transfer 48 (2005) 4598–4614.
[11] A.K. Dhiman, R.P. Chhabra, A. Sharma, V. Eswaran, Effects of Reynolds and Prandtl numbers on the heat transfer across a square cylinder in the steady flow regime, Numer. Heat Transfer A 49 (2006) 717–731.
[12] K.M. Kelkar, S.V. Patankar, Numerical prediction of vortex shedding behind a square cylinder, Int. J. Numer. Methods Fluids 14 (1992) 327–341.
[13] S. Turki, H. Abbassi, S.B. Nasrallah, Two-dimensional laminar fluid flow and heat transfer in a channel with a built-in heated square cylinder, Int. J. Therm. Sci. 42 (2003) 1105–1113.
[14] M. Rahnama, H. Hadi-Moghaddam, Numerical investigation of convective heat transfer in unsteady laminar flow over a square cylinder in a channel, Heat Transfer Eng. 26 (10) (2005) 21–29.
[15] S. Bhattacharyya, S. Mahapatra, Vortex shedding around a heated square cylinder under the influence of buoyancy, Heat Mass Transfer 41 (2005) 824–833.
[16] T.H. Ji, S.Y. Kim, J.M. Hyun, Experiments on heat transfer enhancement from a heated square cylinder in a pulsating channel flow, Int. J. Heat Mass Transfer 51 (2008) 1130–1138.
[17] B. Paliwal, A. Sharma, R.P. Chhabra, V. Eswaran, Power law fluid flow past a square cylinder: momentum and heat transfer characteristics, Chem. Eng. Sci. 58 (2003) 5315–5329.
[18] A.K. Gupta, A. Sharma, R.P. Chhabra, V. Eswaran, Two-dimensional steady flow of a power law fluid past a square cylinder in a plane channel: momentum and heat transfer characteristics, Ind. Eng. Chem. Res. 42 (2003) 5674–5686.
[19] S. Whitaker, Forced convection heat transfer correlations for flow in pipes, past flat plates, single cylinders, single spheres, and for flow in packed beds and tube bundles, AIChE J. 18 (1972) 361–371.
[20] S. Sanitjai, R.J. Goldstein, Forced convection heat transfer from a circular cylinder in cross-flow to air and liquids, Int. J. Heat Mass Transfer 47 (2004) 4795–4805.
[21] R.P. Chhabra, A.A. Soares, J.M. Ferreira, L. Caramelo, Effects of viscous dissipation on heat transfer between an array of long cylinders and power law fluids, Can. J. Chem. Eng. 85 (2007) 808–816.
[22] V. Eswaran, S.A. Prakash, A finite volume method for Navier–Stokes equations, in: Proceedings of the Third Asian CFD Conference, Bangalore, India, vol. 1. 1998, pp. 127–136.
[23] A. Sharma, V. Eswaran, The finite volume method, in: K. Muralidhar, T. Sundararajan (Eds.), Computational Fluid Flow and Heat Transfer, Narosa Publishing, New Delhi, 2003, pp. 445–482.
[24] B.P. Leonard, A stable and accurate convective modeling procedure based on quadratic upstream interpolation, Comput. Meth. Appl. Mech. Eng. 19 (1979) 59–98.
[25] S. Sanitjai, R.J. Goldstein, Heat transfer from a circular cylinder to mixtures of water and ethylene glycol, Int. J. Heat Mass Transfer 47 (2004) 4785–4794.
[26] H.C. Perkins, G. Leppert, Local heat transfer coefficients on a uniformly heated cylinder, Int. J. Heat Mass Transfer 7 (1964) 143–158.